WOOD RESEARCH **doi.org/10.37763/wr.1336-4561/71.2.347362**
e-ISSN 2729-8906
71(2): 2026 347-362 pp.

IN SITU SYNTHESIS OF Mg-Al LAYERED DOUBLE HYDROXIDES IN WOOD: A NOVEL APPROACH FOR ENHANCED FIRE PERFORMANCE

MARTINA HLADOVÁ[1], JOZEF MARTINKA[1], PETER RANTUCH[1], LENKA BLINOVÁ[1], PETER GOGOLA[1], IGOR WACHTER[1], TOMÁŠ ŠTEFKO[1], GEORGE I. MANTANIS[2]
[1]SLOVAK UNIVERSITY OF TECHNOLOGY IN BRATISLAVA, SLOVAK REPUBLIC
[2]UNIVERSITY OF THESSALY, GREECE

(RECEIVED MAY 2026)

ABSTRACT

This study presents a modified approach for enhancing the fire performance of white poplar wood (*Populus alba* L.) through the in situ formation of MgAl layered double hydroxides (LDHs) within the wood structure. The treated wood exhibited significantly improved fire properties. The limiting oxygen index (LOI) increased from 19% to 45%, while cone calorimetry results showed reductions of approximately 65% in peak heat release rate (HRR), 58% in total heat release (THR), 80% in maximum average rate of heat emission (MARHE), and 80% in total smoke production (TSP) compared to untreated poplar wood. The enhanced fire performance is attributed to the formation of a protective char layer and the presence of inorganic residues derived from LDH decomposition, which influences the thermal degradation and combustion behaviour of the wood. The results demonstrate that this simple modification approach provides an effective method for improving the fire performance and smoke suppression properties of fast-growing wood species.

KEYWORDS: Flame retardant, in situ synthesis, Mg-Al layered double hydroxide (LDH), smoke suppressant, wood.

INTRODUCTION

In recent years, the demand for wood has increased as it is used in various industries for its advantages such as a high strength to weight ratio, good thermal insulation properties, low price, renewability, and scalable production (Shen et al. 2024; Hao et al. 2022). However, the supply of high-quality wood is severely insufficient, so the use of fast-growing wood as a substitute for the natural forest because of its high growth rate has become an attractive study in wood applications (Hao et al. 2022). Besides the loose texture and poor mechanical properties, there is a potential fire hazard, which is the key problem in wood utilization. For this

reason, improving the fire performance of fast-growing wood is critically needed (Hao et al. 2022; Kong et al. 2018; Zhang et al. 2022).

Hydrotalcite-like compounds, also named layered double hydroxides (LDHs), are synthetic anionic clays (Lv et al. 2019). LDHs are mainly composed of positively charged hydroxide layers and negatively charged interlayer anions. LDHs have chemical composition tunability and interlayer anion exchangeability, which endow them with unique properties and functions (Yao et al. 2019). The general formula for LDHs is $[M^{2+}_{1-x}\ M^{3+}_{x}(OH)_2]^{x+}\ [(A^{n-})_{x/n}]\cdot mH_2O$, where M^{2+} and M^{3+} are the divalent and trivalent metal cations. A^{n-} is the related anion; and x is the ratio of $M^{3+}/(M^{2+} + M^{3+})$, where $(0.1 < x > 0.5)$ (Altalhi et al. 2024). LDHs are promising eco-friendly flame retardant materials and can retard the growth of flame through three mechanisms. Due to endothermic decomposition LDHs absorb heat, they dilute flammable gases due to releasing water and carbon dioxide, and they decompose to form mixed metal oxides (MMOs) with high specific surface areas, which act as an insulating film on the surface (Sabu and Saju 2024; Lv et al. 2019).

LDHs are extensively studied in polymeric materials for flame-retardant applications. Regarding wood, LDHs were applied through polymeric coatings (Ran et al. 2025; Hu & Sun 2021), or vacuum impregnations (Liu et al. 2024). However, a promising approach appears to be the in situ synthesis in wood. LDHs were created successfully directly in wood via in situ hydrothermal synthesis on paulownia wood with pretreatment step (Lv et al. 2019), two-step in situ synthesis on birch wood (Guo et al. 2017) and urea hydrolysis in Soxhlet apparatus on bamboo wood surface (Yao et al. 2019). All of the mentioned studies showed superior fire performance and smoke suppression effects in comparison to other flame retardants. To the best of our knowledge, in situ growth of MgAl LDHs on poplar wood for flame-retardant applications has not yet been reported. This study, therefore, investigates the flame-retardant properties of MgAl LDHs synthetized in situ on white poplar wood (*Populus alba* L.) using a simplified, modified one-step urea hydrolysis method.

MATERIAL AND METHODS

Samples of white poplar wood (*Populus alba* L.) were purchased from JAF HOLZ Slovakia, s.r.o. (Spačince, Slovakia). Wood samples were dried until constant weight at 103±2°C. Magnesium nitrate $[Mg(NO_3)_2\cdot 6H_2O]$, aluminum nitrate $[Al(NO_3)_3\cdot 9H_2O]$, and urea $[CO(NH_2)_2]$ were purchased from Centralchem s.r.o. (Bratislava, Slovakia). All reagents were used without any further purification. Distilled water was used as the solvent for the preparation of the solutions.

In situ LDH synthesis by urea hydrolysis method

Magnesium nitrate hexahydrate and aluminium nitrate nonahydrate were dissolved in a distilled water at a Mg:Al molar ratio of 2:1, with a total metal ion concentration of 0.6 $mol\cdot L^{-1}$. Urea was added to the solution at a concentration of 3.2 $mol\cdot L^{-1}$. The solution was stirred until complete dissolution of all reagents.

Dried wood samples were placed in a borosilicate glass vessel and were fully covered with the prepared solution. Specimens were kept submerged during the whole synthesis. The vessel

was covered with a glass lid and vacuum impregnated in a vacuum chamber. The impregnation was carried out firstly in a vacuum (absolute pressure ~1 kPa) for 2 h, followed by impregnation at atmospheric pressure for 12 h. The covered vessel with samples was then transferred into a laboratory oven preheated to 120°C and maintained at this temperature for 12 h to promote in situ formation of MgAl LDHs. After the reaction period, the oven was switched off, and the samples were allowed to cool slowly (~10°C·h^{-1}) to room temperature inside the oven overnight. The samples were then removed from the resulting slurry, and excess surface deposits were wiped away. The samples were washed three times with distilled water to remove impurities. The specimens were dried firstly at the room temperature for 48 h, followed by drying at 40±1°C for 24 h and subsequently at 103±2°C until constant weight was achieved.

Characterization of the samples

Untreated poplar wood is denoted as "wood or untreated wood" and treated wood as "MgAl wood or MgAl treated wood". Average densities of untreated wood and MgAl treated wood were 379±6 kg·m^{-3} and 684±11 kg·m^{-3}, respectively.

The sample observation was performed using a JEOL JSM 7600F scanning electron microscope (SEM, Jeol Ltd., Tokyo, Japan) with a Schottky field emission electron source operating at 10 kV. The samples were placed at a working distance of 15 mm and documented using an off-axis backscattered electron detector. The chemical element analysis was performed via an Oxford Instruments X-Max silicon drift detector, energy dispersive X-ray spectrometer (EDS, Oxford Instruments plc, Abingdon, United Kingdom).

Fourier Transform Infrared (FTIR) spectra were acquired using an Agilent Technologies Varian FT-IR Spectrometer 660 (Santa Clara, USA) equipped with a PIKE Technologies GladiATR accessory (Madison, USA). Spectra were collected in the wave number 4000–400 cm^{-1} range with a resolution of 4 cm^{-1} and averaged over 160 scans. The final spectra were corrected for back-ground air absorbance.

Fire performance and thermogravimetric analysis

Fire performance was determined using cone calorimetry (Dual Cone Calorimeter, Fire Testing Technology ltd., East Grinstead, United Kingdom) in accordance with ISO 5660-1 (2015) standard. The heat flux in a horizontal position was set up to 50±0.5 kW·m^{-2}. The samples, with dimensions of (100×100×20) ±1 mm, were conditioned prior to measurement in accordance with the mentioned standard.

Limiting oxygen index (LOI) was measured by device and procedure exactly according to ISO 4589-2 (2017). Samples dimensions were (100×10×4) ±0.2 mm (L×R×T).

For thermogravimetric analysis, Netsch STA 449 F5 Jupiter (Germany, Selb) analyser was used. All samples were measured in inert atmosphere (nitrogen flow rate 100 ml·min^{-1}) at constant heat rate 10°C·min^{-1}. The mass of the sample was 10±0.5 mg.

Mechanical properties

Testing of mechanical properties included three-point bending and Janka hardness test. Three-point bending test was performed with samples in size (100×10×4) ±0.5 mm. The samples were dried at 103±2°C before testing until constant weight. For the Janka hardness

testing, the samples had dimensions of (100×10×4) ±0.5 mm and were conditioned at 50% moisture content and 22°C.

RESULTS AND DISCUSSION

EDX/SEM analysis

In Fig. 1, the elemental composition of the cross-section of the MgAl treated wood sample is presented. In addition to C and O, which are already present in the wood structure, Mg and Al were clearly detected and their distribution throughout the entire analysed region can be observed. Furthermore, the Mg^{2+}/Al^{3+} ratio was found to be close to the theoretical value expected for LDH structures.

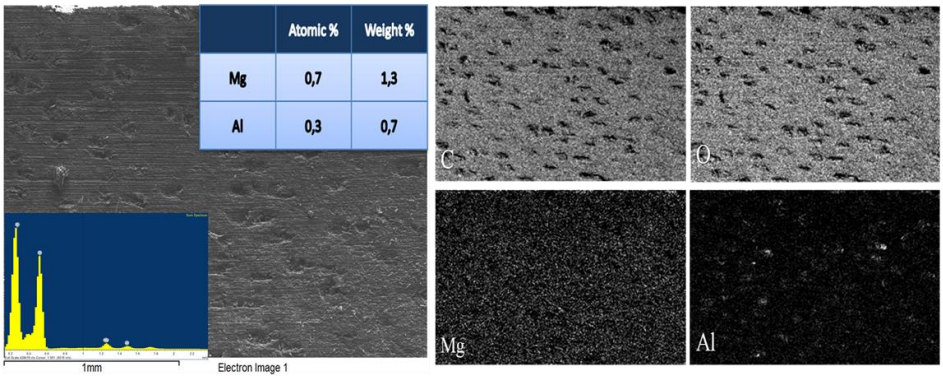

Fig. 1: Elemental analysis of cross section of MgAl treated wood.

However, Fig. 1 suggests that Al was not distributed completely uniformly, as localized regions with higher Al concentration seems to be observed. This behaviour may be attributed to the strong affinity of Al^{3+} ions for carboxyl groups present in the hemicelluloses and pectin in wood, leading to preferential binding in specific structural regions, as was reported by Saito et al. (2014). In contrast, Mg appeared to be more evenly distributed throughout the analysed region. Therefore, local areas exhibiting increased Al-to-Mg ratios were observed, indicating the presence of localized Al dominant regions.

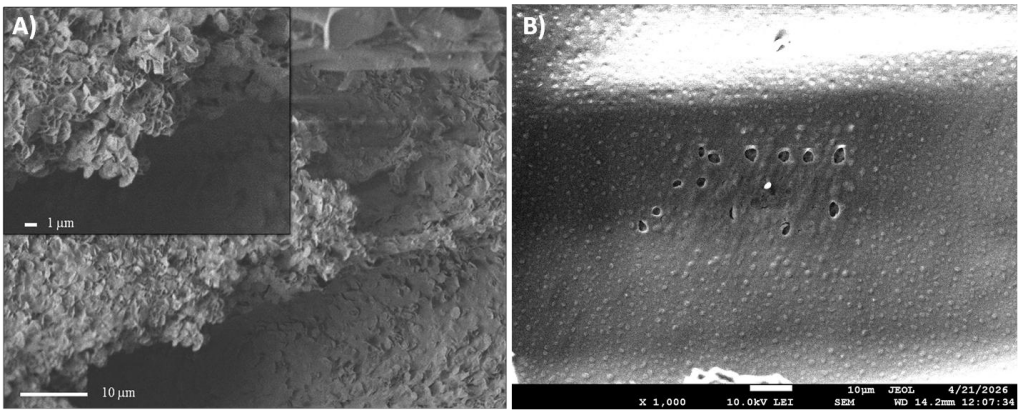

Fig. 2: SEM image of the MgAl treated wood surface (A), and inside of the MgAl wood (B).

In Fig. 2A, there are visible thin, platelet-like structures on the surface of the wood, forming

hierarchical aggregates exhibiting perpendicular orientation, which looks similar to the reported ones in other studies, mainly by Yao et al. (2019), Lv et al. (2019) and Guo et al. (2017). However, these structures were found only on the surface of the wood and similar platelet-like structures weren't find inside of treated wood (Fig. 2B), although EDX analysis confirmed the presence of Mg and Al throughout the whole region. Instead, uniform hemispherical protrusion-like deposits were observed inside the treated wood, suggesting the presence of inorganic material. Overall, the SEM observations indicate that well-defined MgAl LDH particles were predominantly formed on exposed wood surfaces, whereas within the internal structure of the wood, the inorganic coating inside the treated wood is possibly formed.

FTIR-ATR analysis

FTIR-ATR spectroscopy was employed to identify the functional groups present in MgAl LDH, untreated wood, and wood treated by the in situ synthesis of MgAl LDH (Fig. 3).

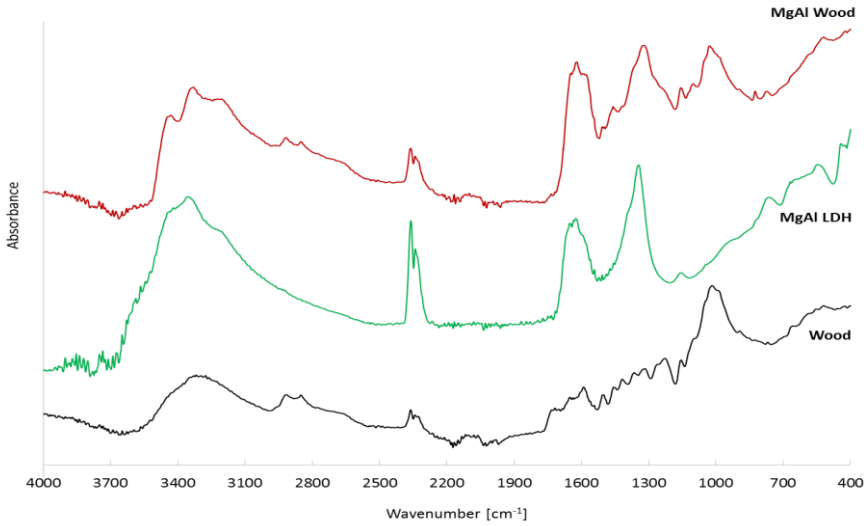

Fig. 3: FTIR spectrum of untreated wood, MgAl treated wood and MgAl LDH.

Untreated wood shows characteristic absorption bands at 3317 cm^{-1} (O–H stretching vibration of cellulosic hydroxyl groups) (Wachter et al. 2026); 2917 and 2850 cm^{-1} (stretching vibrations of C–H bonds in cellulose) (Brisebois et al. 2025); 1718 cm^{-1} (unconjugated C=O stretching in Xylan, a hemicellulose component); 1590 cm^{-1}, 1500 cm^{-1}, and 1418 cm^{-1} (aromatic skeletal vibrations in lignin); 1450 cm^{-1} (C–H deformation coupled with aromatic skeletal vibration); 1360 cm^{-1} (C–H deformation in cellulose and hemicellulose); 1155 cm^{-1} (C–O–C antisymmetric bridge stretching in cellulose and hemicellulose); and 1017 cm^{-1} (C–O stretching mainly in cellulose) (Wachter et al. 2026). An absorption band observed around 2360 cm^{-1} originates from atmospheric CO_2 present during the FTIR measurement (Cao et al. 2022). It is visible in all spectra.

The FTIR spectrum of the prepared MgAl LDH exhibited a broad absorption band in the 3600–3000 cm^{-1} region, which can be attributed to the stretching vibration of the hydroxyl groups in the LDH layers and interlayer water molecules (Peng et al. 2015), or to O─H vibrations of interlayer water associated with interlayer CO_3^{-2} anions (Singh et al. 2020).

A band observed near 1625 cm^{-1} corresponds mainly to the bending vibration of interlayer water molecules (Singh et al. 2020; Peng et al. 2015). Cao et al. (2022) reported that the sample prepared using higher precursor concentrations ($Mg(NO_3)_2$, $Al(NO_3)_3$, and $NaNO_3$) exhibited a band at 1355 cm^{-1} with a shoulder at higher wavenumbers, which was attributed to the co-intercalation of nitrate and carbonate anions. In contrast, the sample synthesized at lower precursor concentrations showed a more distinct band at 1362 cm^{-1} assigned predominantly to intercalated carbonate anions. According to Matusik and Deng (2020), the presence of intercalated NO_3^- in Mg-Al sample was evidenced by a sharp band at 1385 cm^{-1} attributed to N–O stretching vibrations. Roy et al. (2023) assigned the band at 1350 cm^{-1} to the asymmetric stretching vibration mode (ν_3) of nitrate anions, indicating their effective intercalation into the LDH interlayer space. The authors reported that free nitrate anions possess D_3h symmetry, which becomes distorted after intercalation into the LDH interlayer space due to interactions with water molecules and hydroxyl groups. This symmetry distortion was evidenced by the appearance of a weak band around 1030 cm^{-1} corresponding to the symmetric N–O stretching vibration (ν_1), which is normally IR-inactive for free nitrate anions. Additional bands observed at 820 and 667 cm^{-1} were attributed to the ν_2 (out-of-plane bending) and ν_4 (in-plane bending) vibration modes of nitrate anions. According to Benhiti et al. (2020), the carbonate anion in a symmetric environment exhibits D_3h planar symmetry and, similarly to the free carbonate ion, displays three IR-active absorption bands. In most LDHs, these bands are typically observed at approximately 1358 cm^{-1} (ν_3), 873 cm^{-1} (ν_2), and 686 cm^{-1} (ν_4). Based on these literature findings, the absorption band at 1345 cm^{-1} with a shoulder at higher wavenumbers may indicate the presence of intercalated nitrate and/or carbonate anions in the LDH interlayer space. However, the absence of clearly visible characteristic vibrational bands at 1030 cm^{-1}, and in the 820–680 cm^{-1} region does not allow a clear distinction between these two anion types. In the fingerprint region, bands in the range of 800–500 cm^{-1} are attributed to M–O (M is Mg or Al) lattice vibrations within the LDH structure (Singh et al. 2020; Peng et al. 2015; Lv et al. 2019). In particular, Zhang et al. (2019) assigned the peaks at 779 cm^{-1} and 445 cm^{-1} to stretching and bending vibrations of metal–oxygen bonds within the layers, respectively, which is in good agreement with the bands observed in the present study at 763 cm^{-1} and 442 cm^{-1}.

Compared with unmodified wood, the FTIR spectrum of wood modified by the in situ synthesis of MgAl LDH exhibited several noticeable changes. In the 3600–3000 cm^{-1} region, the O–H stretching band shows a slight increase in intensity and a partial splitting into three overlapping maxima. This behaviour may be associated with hydroxyl groups, interlayer water, and intercalated anions in the layered double hydroxide structure, indicating hydrogen-bonding interactions within the wood–LDH system. Significant changes were also observed in the 1800–1580 cm^{-1} region, where the characteristic bands of unmodified wood are no longer visible in the spectra, while a new band appeared at 1622 cm^{-1}. This band is mainly attributed to the bending vibration of interlayer water in the layered double hydroxides structure, suggesting modifications in the hydrogen-bonding environment and possible interactions between the MgAl LDH phase and oxygen-containing functional groups of wood components.

In the LDH treated wood, a new band at 1322 cm^{-1} was detected, whereas the characteristic hemicellulose- and cellulose-related bands in this region became less distinct. This band can be assigned to intercalated nitrate or carbonate anions in the LDH interlayer space. Absorption at

1028 cm^{-1} cannot be attributed to nitrate anions in LDH as it may be overlapped by the band already present in that region in the pristine wood, which represents C–O stretching and aromatic C–H in plane deformation from cellulose and lignin (Zhuang et al. 2020; Li et al. 2015). The band observed at 823 cm^{-1} can be attributed to the υ2 out-of-plane bending mode of nitrate anions, which was reported near 820 cm^{-1} by Roy at al. (2023). Finally, the region below 800 cm^{-1} is dominated by M–O lattice vibrations (M = Mg, Al), confirming the presence of the LDH phase within the wood structure.

The absorption bands characteristic of NO_3^- cannot be clearly distinguished in the spectrum because the vibrations of CO_3^{2-} occur at similar wavenumbers (Lange et al. 2015; Zhang et al. 2019). The CO_3^{2-} bands in the spectrum may originate from atmospheric CO_2 as well as from CO_2 released during urea decomposition throughout the MgAl LDH preparation process.

TG and DTG analysis

Summary results of thermogravimetry (TG) and derivative thermogravimetry (DTG) of wood, MgAl treated wood and pure MgAl LDH are presented in Tab. 1.

Tab. 1: Results of thermogravimetric analysis of wood, MgAl treated wood and MgAl LDH.

Sample		Wood	MgAl LDH	MgAl wood
1st region	Range [°C]	< 120	< 119	< 118
	T_{max} [°C]	65.3	74.3	60.4
	Weight loss [%]	1.6	3.1	2.3
2nd region	Range [°C]	178 - 480	119 - 288	118 – 261
	T_{max} [°C]	339.8	226	219.7
	Weight loss [%]	74.7	32.6	28.2
3th region	Range [°C]	-	288 – 585	261 – 392
	T_{max} [°C]	-	302.8 388.8 474.5	328.3
	Weight loss [%]	-	20.1	28.9
4th region	Range [°C]	> 480	> 585	> 392
	T_{max} [°C]	-	-	-
	Weight loss [%]	5.1	1.3	13.8
Residue at 800°C [%]		18.3	42.8	26.6

Fig. 4 shows TG and DTG curves of the untreated wood and MgAl treated wood sample. The thermal decomposition of untreated wood can be categorized into three main stages. The first stage of mass loss in untreated wood was observed at temperatures up to 120°C. This phenomenon is common in lignocellulosic materials and is caused by the reduction of moisture content in the samples (Xing & Li 2014; Fraga et al. 2020; Ochieng et al. 2023). This moisture was absorbed by the samples from the surrounding air during handling prior to the measurement.

The main mass loss occurs in the second stage. Thus is caused by the decomposition of hemicelluloses, cellulose, and partially also lignin. Yang et al. (2007) reported that, in a nitrogen atmosphere, the main decomposition of hemicelluloses occurs in the temperature range of 220–315°C, cellulose occurs between 315–400°C, and lignin occurs over a broad range from 160°C to 900°C. The peak corresponding to the decomposition of hemicelluloses is overlapped on the DTG curve (Fig. 4B) by the decomposition of cellulose. Therefore, it appears only as a shoulder around 285°C, which is consistent with the results reported by Sebio-Punal et

al. (2012) who reported values around 280°C for several wood species. Among the components present in wood, cellulose is the most significant. Poplar wood contains approximately 50–53% cellulose (Krutul et al. 2019). At the same time, its decomposition rate is significantly higher compared to hemicelluloses and lignin, and it decomposes almost completely without residue (Yang et al. 2007). For these reasons, the main decomposition peak observed at approximately 340°C can be attributed to cellulose.

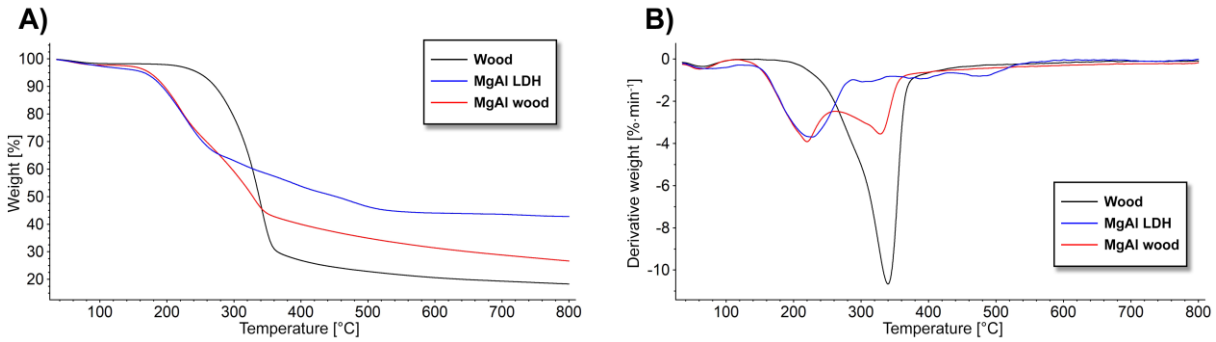

Fig. 4: TG (A) and DTG (B) of untreated wood, MgAl treated wood and MgAl LDH.

Compared to the carbohydrate fraction of wood, lignin decomposes more slowly and over a broad temperature range. Therefore, it is not clearly visible on the TG and DTG curves and is manifested only by a relatively slow mass loss after the completion of cellulose decomposition (Abdo et al. 2024). This region was observed at temperatures above 390°C.

In the final stage, the carbon-rich residue undergoes slow decomposition, accompanied by the release of a low amount of volatile compounds (Almusafir & Smith 2024). The final mass is non-zero due to the presence of fixed carbon and ash (Cisse et al. 2022).

The mass loss of MgAl LDH can be divided into four regions. The first region, up to 119°C, is, similarly to untreated wood, caused by moisture evaporation (Lv et al. 2019). In the second region, with a peak at 226°C, structural water is released from the MgAl LDH structure (Yao et al. 2019; Guo et al. 2017). During the third stage, a gradual decomposition occurs; however, the corresponding DTG curve shows several small peaks, which appear to be related to at least three minor decomposition processes. These can be related to thermal decomposition of interlayered anions and dihydroxylation (Zhao et al. 2015; Yao et al. 2019). In the final fourth stage, the residue remains practically constant, without further detectable reactions.

The MgAl treated wood sample also exhibits four stages of mass loss during TGA. In the first stage, as in the other cases, drying of the sample occurs. This is followed by a decomposition stage that is practically identical to that of MgAl LDH. This suggests that while wood components are still thermally stable at lower temperatures, the main contributor to decomposition is the presence of MgAl LDH. During this stage MgAl LDH releases a large amount of crystal water and adsorbed water (Yao et al. 2019). In this step, Lv et al. (2019) and Guo et al. (2017) report also the decomposition of hemicellulose, and Lv et al. (2019) also reports the conversion of CO_3 to CO_2.

The third stage differs from both MgAl LDH and untreated wood. This can be explained by the interaction of the applied flame retardant with wood components, especially cellulose, whose decomposition plays a key role in this region. Due to the reduced decomposition rate, it

can be assumed that MgAl LDH thermally stabilizes part of the cellulose chain. It is also possible that char-forming or cross-linking reactions occur (Lv et al 2019), which contribute to the altered degradation behaviour. It is also reported by Guo et al. (2017), that from 280°C to 380°C, thermotropic phase transition of MgAl LDH to diaspore and brucite structures occurs. Also, in this stage dihydroxylation of the LDH occurs (Lv et al. 2019). In the final stage, similarly to untreated wood, only a slow decomposition of the carbonized residue takes place. Char residue increased from 18.3% for untreated wood to 266% for treated MgAl wood sample.

Fire performance

The results shows that the LOI of treated MgAl wood sample increased from 20% to 45% in comparison with untreated wood. This shows the significant improvement in resistance to ignition. Similar results were observed by Guo et al. (2017), where the LOI improved to 39 % and by Lv et al. (2019), with the LOI improvement to 48%.

Fire performance of the treated MgAl wood sample was further evaluated by cone calorimetry, where untreated wood was measured as a reference. Heat Release Rate (HRR), Smoke Production Rate (SPR), CO Release Rate and Mass Loss Rate (MLR) were measured. From these base characteristics the derived parameters were obtained, mainly: Effective Heat of Combustion (EHC), Total Heat Release (THR), Total Smoke Production (TSP), Specific Smoke Extinction Area per mass loss (SEA_m), Specific Smoke Extinction Area per released heat (SEA_q), Total CO Production (TCOP), Carbon Monoxide Yield per mass loss (CO_m), Carbon Monoxide Yield per released heat (CO_q), and Residue Mass (RM).

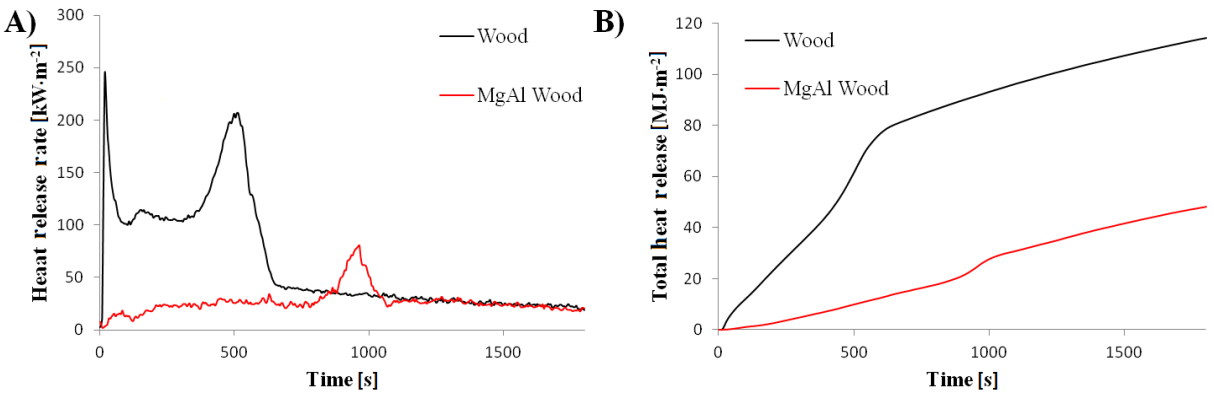

Fig. 5: HRR (A) and THR (B) of MgAl treated wood and untreated wood.

HRR refers to the amount of heat release from the specimen per unit area under a constant imposed heat flux, and the peak-HRR value is generally used to express fire intensity. THR represents the cumulative amount of the heat released by the material from ignition until a specified time under predetermined incident heat flow intensity. The higher HRR and THR, the more heat generated, resulting in faster material pyrolysis and increased production of volatile combustibles, thus accelerating flame propagation (Cheng et al. 2022; Tan et al. 2024).

Fig. 5A shows the HRR of untreated and treated MgAl wood. For the untreated wood, there are two peaks, which is in agreement with other results for poplar wood (Cheng et al. 2022). The first peak generally corresponds to the transient flaming combustion that occurs upon sample ignition (Tan et al. 2024) and can be associated with the oxidation and degradation of

volatile pyrolysis products of wood components, and the rapid carbonization process (Pan et al. 2025) immediately after ignition. The second peak is a response to sample burn through, meaning that the heat gradient reaches the rear side of the sample, where the rear insulator material limits heat dissipation and raises the temperature and pyrolysis rate of the entire sample (Sanned et al. 2023). As shown in Fig. 5, it can be seen, that this simplified method of MgAl treatment caused major decrease of HRR, and MgAl wood sample showed only one distinct peak at around 900 s. This may be explained by the flame retardant effect of MgAl LDH, which releases H_2O and CO_2/NO_3 and forming mixed metal oxides (MMO) during decomposition, thereby diluting combustible gases and absorbing heat to reduce heat release and minimizing amount of fuel available for propagating reaction (Guo et al. 2017). Also, the metal oxides contribute to the formation of a char layer, which may limits the heat and mass transfer, delaying the ignition time and thereby shifting the first distinct peak to a later time.

In the Fig. 5B, it can be seen that THR was decreased in about 58%. Similar results were shown by Lv et al. (2019).

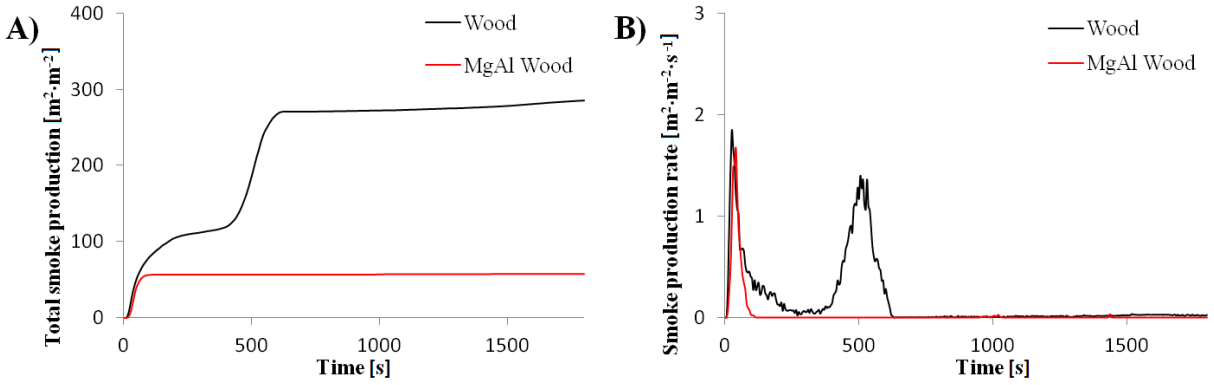

Fig. 6: TSP (A) and SPR (B) of untreated wood and MgAl treated wood.

The large amount of smoke produced in the early stages of a fire is very harmful, because smoke comprised of carbon particles can diminish visibility (Guo et al. 2017). As shown in the Fig. 6A, it is clearly visible, that MgAl wood caused significant decrease of the TSP (~80%). The SPR in the Fig. 6B is showing that the MgAl treated wood is producing the smoke mainly during the first stages of the combustion process. Initial smoke production peak of MgAl wood is slightly lower than untreated wood (1.67 $m^2 \cdot m^{-2} \cdot s^{-1}$ vs 1.84 $m^2 \cdot m^{-2} \cdot s^{-1}$, respectively) and then significantly decrease without any further obvious rises.

In the Fig. 7A, it can be seen, that the MgAl treated wood did not have any obvious effect on total CO production. However, as it can be seen from Fig. 7B, the CO production rate started increasing in a slightly later time then untreated wood. Although it reached higher value in the beginning of the test compared to untreated wood, then it stayed approximately in the same level and after about 1000s, it started to decrease. This may be caused by the decomposition products of LDH, which can insulate the heat and prevent atmospheric oxygen from contacting the protected materials (Lv et al. 2019), leading to incomplete combustion. Both CO (Fig. 7) and smoke (Fig. 6) are products of incomplete combustion. MgAl treatment significantly reduces TSP at the expense of the immediately CO production rate (between ~200 to ~1000 s).

However, since the total CO production remains unchanged, MgAl treatment effectively improves combustion efficiency.

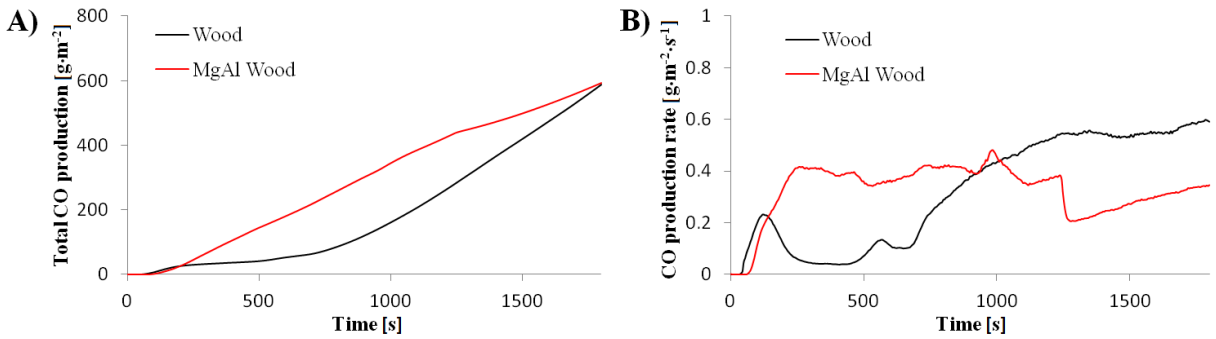

Fig. 7: Total CO production (A) and CO production rate (B) of untreated wood and MgAl treated wood.

In untreated wood, flaming combustion ends at about 600 s (Fig. 5A), following the smouldering phase during which the maximum CO production rate is observed (Fig. 7B). In contrast, ignition of the MgAl treated sample occurs only at around 1000 s, after which the CO production rate gradually decreases (Fig. 7B). This behaviour can be attributed to the flame-retardant effect of MgAl treatment, which significantly increases the time to ignition. During the period between thermal exposure and ignition, the formation of incomplete combustion products is typically the most intensive. At the same time, the low smoke production of the MgAl treated sample after the initial SPR peak (Fig. 6B) further suggests that thermal degradation and combustion of the treated wood predominantly release gaseous products of incomplete combustion rather than particulate smoke components.

In the Tab. 2, the overview of the main fire characteristics of untreated and MgAl treated wood is presented. The statistical significance of the differences in fire performance between wood and MgAl wood was evaluated using Duncan's test at a significance level of $\alpha = 0.05$. The obtained results demonstrate that MgAl wood exhibits improved fire performance characteristics in comparison to wood, which is statistically significant in all cases (higher TTI values, indicating increased ignition resistance; higher RM values, indicating improved fire resistance; and lower values for all other parameters), except for TCO, where the difference is statistically insignificant. This is a very interesting result because only a few flame retardants improve almost all fire characteristics without worsening any others.

The relationship between RM (Tab. 2) and wood charring rate is described e.g. by Martinka et al. (2018). The charring rate represents an important fire characteristic that determines the fire resistance of wood timbers. More detailed information on wood charring is available in scientific papers such as Parnicanova et al. (2024).

Tab. 2: Fire performance of MgAl treated and untreated poplar wood.

Property / Sample [-]	Wood	MgAl Wood
TTI [s]	13±2	988±249
MARHE [kW·m^{-2}]	136±2	29±10
HRR$_{max}$ [kW·m^{-2}]	254±21	87±40
THR [MJ·m^{-2}]	114±2	48±13

EHC [MJ·kg^{-1}]	14±0.5	3.85±0.93
RM [%]	4.87±0.07	19.62±0.89
TCO [g·m^{-2}]	587±55*	592±171*
COY$_m$ [g·kg^{-1}]	71.84±7.76	47.55±14.29
COY$_q$ [g·MJ^{-1}]	5.12±0.36	13.09±5.59
TSP [m^2·m^{-2}]	286±59	57±6
SEA$_m$ [m^2·kg^{-1}]	35.05±7.70	4.61±0.56
SEA$_q$ [m^2·MJ^{-1}]	2.49±0.46	1.26±0.37

Note: TTI: time to ignition, MARHE: maximum average rate of heat emission, HRR_{max}: maximum heat release rate, THR: total heat release, EHC: effective heat combustion, RM: residue mas, TCO: Total CO released, COY_m: carbon monoxide yield per mass loss, COY_q: carbon monoxide yield per release heat, SEA_m: Smoke extinction area per mass loss, SEA_q: smoke extinction area per release heat. Upper indexes * in the one row indicate values *p* values of Duncan´s test higher than 0.05 – no statistically significant difference.

Mechanical properties

Tab. 3 presents the results of the mechanical tests performed on pristine wood and MgAl treated wood samples. The three-point bending test revealed a decrease in the modulus of rupture of the MgAl treated samples compared to untreated wood. A similar trend was also observed in the Janka hardness test. These results indicate that the MgAl treatment negatively affected the mechanical properties of poplar wood. Similar findings were reported by Lv et al. (2019), who also observed a reduction in the mechanical properties of paulownia wood following in situ LDH formation.

Tab. 3: Selected mechanical properties of untreated wood and AlMg treated wood.

Sample	Modulus of rapture [MPa]	Janka hardness [N·mm^{-2}]
Wood	88.08±14.78	15.10±0.18
MgAl Wood	41.54±1.56	7.83±0.18

CONCLUSIONS

In this study, a simplified in situ synthesis route for MgAl LDHs in poplar wood was investigated. SEM analysis revealed the presence of characteristic hexagonal LDH platelets on the wood surface. Despite the simplified synthesis procedure, the resulting MgAl based flame retardant exhibited excellent fire-retardant performance. The limiting oxygen index (LOI) increased from 20% for untreated wood to 45% for MgAl treated wood. Cone calorimetry results indicated that the MgAl treatment effectively suppressed heat release and smoke generation during combustion, while also delaying ignition. However, the MgAl treatment negatively affected the mechanical properties of the wood, resulting in a reduced modulus of rupture and lower surface hardness compared to untreated poplar wood.

ACKNOWLEDGMENTS

This work was supported by the Slovak Research and Development Agency under the Contract no. APVV-24-0143. This work was also supported by the VEGA agency for the project VEGA 1/0755/25.

REFERENCES

1. Abdo, M., Flity, H., Terrei, L. et al. (2024). An alternative wood pyrolysis model based on TGA and cone calorimeter tests. *Thermochimica Acta* 731: e179646.
2. Almusafir, R., Smith, J.D. (2024). Thermal decomposition and kinetic parameters of three biomass feedstocks for the performance of the gasification process using a thermogravimetric analyzer. *Energies* 17(2): e396.
3. Altalhi, A.A., Mohamed, E.A., Negm, N.A. (2024). Recent advances in layered double hydroxide (LDH)-based materials: fabrication, modification strategies, characterization, promising environmental catalytic applications, and prospective aspects. *Energy Advances* 3(9): 2136-2151.
4. Benhiti, R., Ichou, A.A., Zaghloul, A. et al. (2020). Synthesis, characterization, and comparative study of MgAl-LDHs prepared by standard coprecipitation and urea hydrolysis methods for phosphate removal. *Environmental Science and Pollution Research* 27: 45767-45774.
5. Brisebois, P., Aouinti, M., Jafari, M. et al. (2025). Adsorption dynamics of disodium octaborate tetrahydrate on clay minerals: implications for construction wood protection. *Small Methods* 9: e2400753.
6. Cao, Y., Fang, S., Chen, K. et al. (2022). Insight into the preparation of MgAl-layered double hydroxide (LDH) intercalated with nitrates and chloride adsorption ability study. *Applied Sciences* 12: e4492.
7. Cheng, X., Lu, D., Yue, K. et al. (2022). Fire resistance improvement of fast-growing poplar wood based on combined modification using resin impregnation and compression. *Polymers* 14(17): e3574.
8. Cisse, I., Hernandez-Charpak, Y.D., Diaz, C.A., Trabold, T.A. (2022). Biochar derived from pyrolysis of common agricultural waste feedstocks and co-pyrolysis with low-density polyethylene mulch film. *Waste and Biomass Valorization* 13(9): 3913-3932.
9. Fraga, L.G., Silva, J., Teixeira, S. et al. (2020). Thermal conversion of pine wood and kinetic analysis under oxidative and non-oxidative environments at low heating rate. *Proceedings* 58(1): e23.
10. Guo, B., Liu Y., Zhang Q. et al. (2017). Efficient flame-retardant and smoke-suppression properties of Mg–Al-layered double-hydroxide nanostructures on wood substrate. *ACS Applied Materials & Interfaces* 9(27): 23039-23047.
11. Hao, X., Li, M., Huang, Y. et al. (2022). High-strength, dimensionally stable, and flame-retardant fast-growing poplar prepared by ammonium polyphosphate–waterborne epoxy impregnation. *ACS Applied Polymer Materials* 4(2): 1305-1313.
12. Hu, X., Sun, Z. (2021). Nano $CaAlCO_3$-layered double hydroxide-doped intumescent fire-retardant coating for mitigating wood fire hazards. *Journal of Building Engineering* 44: e102987.
13. ISO 4589-2. (2017). Plastics. Determination of burning behaviour by oxygen index. Part 2: Ambient-temperature test.

14. ISO 5660-1. (2015). Reaction to fire tests. Heat release, smoke production and mass loss rate. Part 1: Heat release rate (cone calorimeter method) and smoke production rate (dynamic measurement).
15. Kong, L., Guan, H., Wang, X. (2018). In situ polymerization of furfuryl alcohol with ammonium dihydrogen phosphate in poplar wood for improved dimensional stability and flame retardancy. *ACS Sustainable Chemistry & Engineering* 6(3): 3349-3357.
16. Krutul, D., Antczak, A., Kłosińska, T. et al. (2019) The chemical composition of poplar wood in relation to the species and age of trees. *Annals of Warsaw University of Life Sciences SGGW Forestry and Wood Technology* 105: 125-132.
17. Lange, C.-E., Lastusaari, M., Reza, M. et al. (2015). In Situ hybridization of pulp fibers using Mg-Al layered double hydroxides. *Fibers* 3: 103-133.
18. Li, G., Lao, W., Qin, T., Huang, L. (2015). Rapid determination of biomass and polypropylene in three types of wood plastic composites (WPCs) using FTIR spectroscopy and partial least squares regression (PLSR). *Holzforschung* 69(4): 399-404.
19. Liu, X., Wang, Z., Chen, M. et al. (2024). Phytic acid/cellulose nanofibers modified layered double hydroxides flame retardants: Synthesis, properties and applications. *International Journal of Biological Macromolecules* 283: e137562.
20. Lv, S., Kong, X., Wang, L. et al. (2019). Flame-retardant and smoke-suppressing wood obtained by the in situ growth of a hydrotalcite-like compound on the inner surfaces of vessels. *New Journal of Chemistry* 43: 16359-16366.
21. Martinka, J., Rantuch, P., Liner, M. (2018). Calculation of charring rate and char depth of spruce and pine wood from mass loss. *Journal of Thermal Analysis and Calorimetry* 132(2): 1105-1113.
22. Matusik, J., Deng, Y. (2020). Fumonisin B_1 interaction with Mg-Al and Mg-Fe layered double hydroxides: removal efficiency and mechanisms. *Materials* 13: e4344.
23. Ochieng, R., Cerón, A.L., Konist, A., Sarker, S. (2023). A combined analysis of the drying and decomposition kinetics of wood pyrolysis using non-isothermal thermogravimetric methods. *Energy Conversion and Management: X* 20: e100424.
24. Pan, F., Chen, Z., Huang, Y. (2025). Experimental evaluation of combustion performance in the three main anatomical sections of poplar wood. *Wood Material Science & Engineering 20*(1): 11-19.
25. Parnicanova, A., Zachar, M., Kacikova, D. (2024). The influence of the heat flux of the infrared heater on the charring rate of spruce wood. *Polymers* 16(18): 2657.
26. Peng, Y., Wang, W., Cao, J., Guo, X. (2015). Effects of a layered double hydroxide (LDH) on the photostability of wood flour/polypropylene composites during UV weathering. *RSC Advances* 5: 41230-41237.
27. Ran, Y., Ding, J., Yang, F. et al. (2025). A novel organic-inorganic composite flame-retardant coating with excellent compatibility provides superior flame retardancy and smoke suppression for wood. *Industrial Crops and Products* 224: e120286.
28. Roy, A.S., Pillai, S.K., Ray, S.S. (2023): A comparison of nitrate release from Zn/Al-, Mg/Al-, and Mg−Zn/Al layered double hydroxides and composite beads: utilization as slow-release fertilizers. *ACS Omega* 8(9): 8427-8440.

29. Saito, K., Watanabe, Y., Matsushita, Y. et al. (2014). Aluminum localization in the cell walls of the mature xylem of maple tree detected by elemental imaging using time-of-flight secondary ion mass spectrometry (TOF-SIMS). *Holzforschung* 68(1): 85-92.
30. Sanned, E., Mensah, R.A., Försth, M., Das, O. (2023). The curious case of the second/end peak in the heat release rate of wood: A cone calorimeter investigation. *Fire and Materials*, 47(4): 498-513.
31. Sebio-Punal, T., Naya, S., Beceiro, J.L., Tarrío-Saavedra, J. (2012) Thermogravimetric analysis of wood, holocellulose, and lignin from five wood species. *Journal of Thermal Analysis and Calorimetry* 109(3): 1163-1167.
32. Shen, H., Liu, Y., Wang, P. et al. (2024). Preparation of multifunctional flame retardant composite wood by doping poplar cell walls with metal phytates. *Cellulose* 31(15): 9435-9454.
33. Singh, M., Somvanshi, D., Singh, R.K. (2020). Functionalized polyvinyl chloride/layered double hydroxide nanocomposites and its thermal and mechanical properties. *Journal of Applied Polymer Science* 137(27): e 48894.
34. Tan, K., Wang, Y., Li, X. et al. (2024). Surface layer reinforcement modification for wood with high strength and flame retardancy performances. *Construction and Building Materials* 450: e138672.
35. Sabu, T., Saju, D. (2024). Layered double hydroxides: fundamentals to applications. In: Layered double hydroxide polymer nanocomposites (ed. Sabu, T., Saju, D.). Woodhead Publishing. Cambridge. 1-76 pp.
36. Wachter, I., Kvorková, V., Štefko. T. et al. (2026). Green flame retardancy: biomass-based treatment for poplar wood. *European Journal of Wood and Wood Product* 84: e57.
37. Xing, D., Li, J. (2014). Effects of heat treatment on thermal decomposition and combustion performance of Larix spp. wood. *BioResources* 9(3): 4274-4287.
38. Yang, H., Yan, R., Chen, H. et al. (2007). Characteristics of hemicellulose, cellulose and lignin pyrolysis. *Fuel* 86(12-13): 1781-1788.
39. Yao, X., Du, C., Hua, Y. et al. (2019). Flame-retardant and smoke suppression properties of nano MgAl-LDH coating on bamboo prepared by an in situ reaction. *Journal of Nanomaterials*, 2019(1): e9067510.
40. Zhang, L., Zhang, W., Peng, Y. et al. (2022). Thermal behavior and flame retardancy of poplar wood impregnated with furfuryl alcohol catalyzed by boron/phosphorus compound system. *Industrial Crops and Products* 176: e114361.
41. Zhang, W., Li, J., Wang, Y. et al. (2019): Layer-by-layer assembly of luminescent ultrathin films by layered double hydroxides and neutral Al–Phen–Hq. *Research on Chemical Intermediates* 45: 2515-2527.
42. Zhao, X., Zhou, C., Han, B. et al. (2015). Growth mechanism of curved Mg–Al–CO 3 layered double hydroxide nanostructures in a one-pot assembly procedure under ambient pressure. *RSC Advances* 5(26): 19955-19960.
43. Zhuang, J., Li, M., Pu, Y. et al. (2020): Observation of potential contaminants in processed biomass using Fourier transform infrared spectroscopy. Applied Sciences 10(12): e4345.

MARTINA HLADOVÁ, JOZEF MARTINKA*, PETER RANTUCH, LENKA BLINOVÁ,
PETER GOGOLA, IGOR WACHTER, TOMÁŠ ŠTEFKO
SLOVAK UNIVERSITY OF TECHNOLOGY IN BRATISLAVA
FACULTY OF MATERIALS SCIENCE AND TECHNOLOGY IN TRNAVA
JANA BOTTU 25, SK 917 24 TRNAVA
SLOVAK REPUBLIC
*Corresponding author: jozef.martinka@stuba.sk

GEORGE I. MANTANIS
UNIVERSITY OF THESSALY
DEPARTMENT OF FORESTRY, WOOD SCIENCES AND DESIGN
11–13 V. GRIVA STREET, 43100 KARDITSA
GREECE